Flexible and Printed Electronics

PAPER

Printable materials for printed perovskite solar cells

Wangnan Li[1]**, Zhicheng Zhong**[1]**, Fuzhi Huang**[2]**, Jie Zhong**[2]**, Zhiliang Ku**[2]**, Wei Li**[2]**, Junyan Xiao**[2]**, Yong Peng**[1,2] **and Yi-Bing Cheng**[2]

1 Hubei Key Laboratory of Low Dimensional Optoelectronic Materials and Devices, Hubei University of Arts and Science, Xiangyang, People's Republic of China
2 State Key Laboratory of Advanced Technology for Materials Synthesis and Processing, Wuhan University of Technology, Wuhan, People's Republic of China

E-mail: yongpeng@whut.edu.cn

Keywords: perovskite, solar cells, printable materials, flexibility

Abstract

Since its introduction in 2009, the power conversion efficiency of the perovskite solar cell (PSC) has increased from about 3% at the beginning to 24.2% at present, which means that it is the fastest developing new-generation solar cell. However, there are still some bottlenecks to be overcome for its industrialization, including in both materials and fabricating technologies. In this paper, research progress and the existing problems of PSC-related materials which have been used for printing in recent years were reviewed. The characteristics, improvement and optimization of various new materials were introduced in detail. Finally, the research prospects of printing large-area PSCs, improving device stability and reducing fabricating costs were pointed out, which provide some suggestions for future research on printing efficient and stable PSCs.
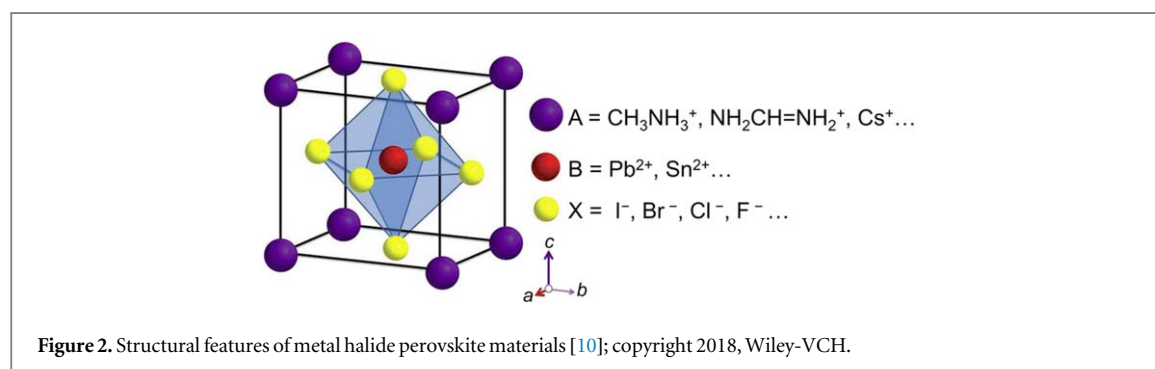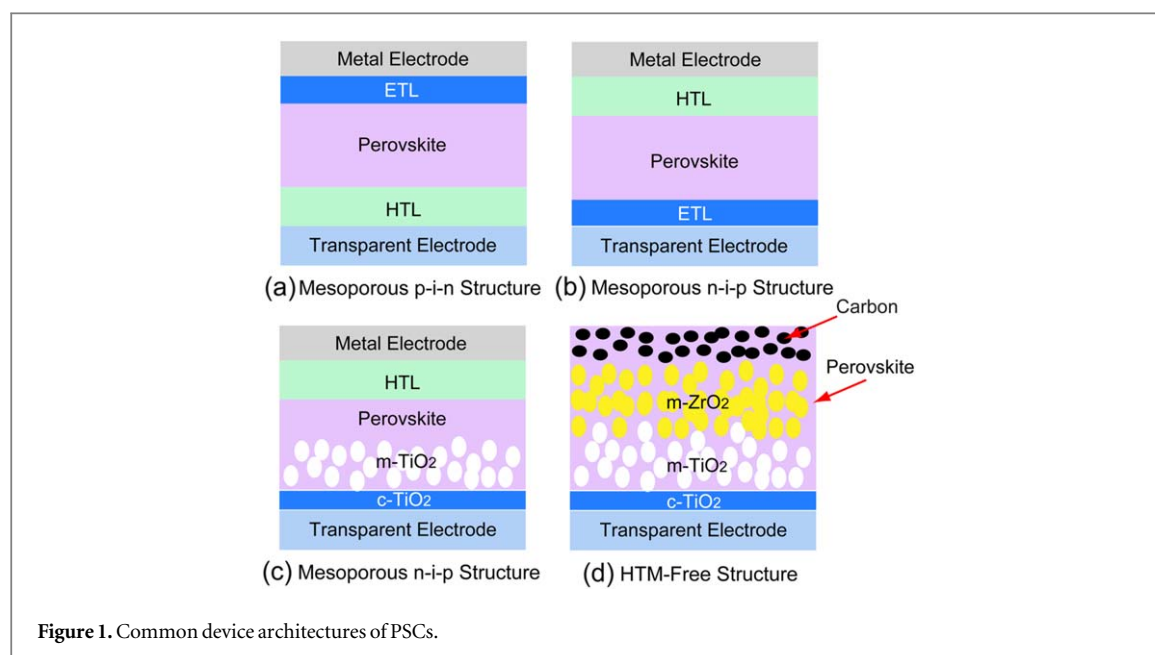
1. Introduction

Perovskite solar cells (PSCs) [1], which are characteristically flexible, light-weight and which have a high power conversion efficiency (PCE), have made great progress in the past few years, and have been widely utilized by researchers and people in the industry [2–7]. The PSC is considered to be an outstanding example of a new-generation cheap solar cell. At present, the internationally notarized PCE of PSCs has exceeded 25.2% [8], and it has certain advantages in terms of material costs and fabrication costs. However, the common technique for preparing high-efficiency PSCs is spin coating, which is simple in operation, fast in film formation and good in repeatability, but which is not desirable for continuous industrial productions.

Printing technologies can not only overcome the shortcomings of the traditional preparation method of PSCs, but they also have the advantages of a high material utilization rate, low costs, the large scale of production, and the adaptability of the flexible substrate; they are thus considered the best preparation technologies for this new-generation, thin film solar cell. However, the wide application of printed PSCs is limited by the large-area low reproducibility of PCE, as well as the poor stability and toxicity of printed devices [9].

In order to promote the industrialization of flexible PSCs, it is vital to urgently develop highly efficient, stable, environmentally friendly and highly adaptable printed PSC inks. In this paper, the ink research and properties of PSCs suitable for printing were introduced, and the important role of the industrialization of PSCs in the development of flexible electronics was discussed.

2. Common materials for the preparation of PSCs

Generally, PSCs have the architectures of a of p-i-n structure, a n-i-p structure and a hole-free structure (as shown in figures 1(a)–(d)). Although structurally different, the PSCs typically consist of five layers: a transparent electrode, an electron transport layer (ETL), a perovskite layer, a hole transport layer (HTL), and a metal electrode, each of which plays an important role in the photovoltaic process. The perovskite layer is the active layer that absorbs sunlight and generates free charges. To prevent charge recombination, the ETL (or HTL) extracts electrons (or holes) from the perovskite and delivers them to the cathode (or anode). In addition, the two intermediate layers should be matched with the perovskite layer to compensate for the energy mismatch between the

Figure 1. Common device architectures of PSCs.

Figure 2. Structural features of metal halide perovskite materials [10]; copyright 2018, Wiley-VCH.

active layer and the electrode. Table 1 shows some common abbreviations of PSCs and their meanings.

2.1. Perovskite materials

In the PSCs, perovskite materials play a role in absorbing incident light, so the photoelectric property of the materials directly influences the photovoltaic characteristics of the device. The perovskite absorption layer is a kind of organic-inorganic hybrid perovskite material. The crystal structure of perovskite can transfer among the tetragonal, cubic and rhombic crystal systems under different temperatures, electric field intensity and pressure conditions. The typical crystal structure is ABX_3, as shown in figure 2.

In the above, A generally refers to organic amine ions such as $CH_3NH_3^+$, $NH = CHNH_3^+$, which are located at the eight vertices of the cube. B is a bivalent metal ion, such as Pb^{2+} and Sn^{2+}, occupying the center of the cube. At the center of the hexahedral surface is the halogen atom X, which is generally doped with I^-, Br^-, Cl^- or a variety of halogens. In contrast to previous hybridization categories, this organic-inorganic hybridization is an integration on the molecular scale, and remains homogeneous at the macro level, which preserves the

Table 1. Abbreviation contrast of PSCs.

No.	abbreviations	Full name
1	PSCs	Perovskite solar cells
2	MPSCs	Mesoporous perovskite cells
3	C-PSCs	Carbon-based perovskite solar cells
4	F-PSCs	Flexible perovskite solar cells
5	PSCMs	Perovskite solar cells modules
6	PSK	Perovskite
7	PCE	Power conversion efficiency
8	ETL/M	Electron transport layer/materials
9	HTL/M	Hole transport layer/materials
10	M-TiO$_2$	Mesoporous titanium oxide
11	C-TiO$_2$	Compact titanium oxide
12	FTO	Fluorine-doped SnO_2 transparent conductive glass
13	ITO	Indium tin oxide
14	PET	Polyethylene terephthalate

performance advantages of inorganic and organic materials while hybridizing and compounding materials [11–13]. The basic properties of the most commonly used perovskite materials are shown in table 2.

The presence of organic group ions makes perovskite more easily soluble in organic solvents for

Table 2. The energy levels of several common perovskite materials [14, 15].

Composition	Bandgap (eV)	Structure at room temperature	Conduction band (CB) (eV)	Valence band (VB)(eV)
$CH_3NH_3PbI_3$	$1.5 \sim 1.61$	Tetragonal	-3.93	-5.3
$CH_3NH_3PbBr_3$	2.32	Cubic	-3.36	-5.58
$CH_3NH_3PbCl_3$	3.1	Cubic	-3.36	-5.58
$CH_3NH_3PbI_{3-x}Cl_x$	$1.55 \sim 1.64$	Tetragonal	-3.75	-5.43
$CH_3NH_3PbI_{3-x}Br_x$	$1.55 \sim 2.32$	Tetragonal/Cubic	-3.75	-5.43
$HC(NH_2)_2PbI_3$	1,47	Tetragonal	-4.2	-5.7
$HC(NH_2)_2PbBr_3$	2.23	Cubic	-4.2	-5.7

convenient preparation, and the properties of perovskite materials can also be optimized by adjusting the size of the organic ions. Common regulation of element A includes mutual substitution and doping among methylammonium (MA, $CH_3NH_3^+$), formamidinium (FA, $CH_3(NH_2)_2^+$) and cesium ions (Cs^+). For example, Lee *et al* [16] synthesized $HC(NH_2)_2PbI_3$ as the light absorption layer of PSCs by substituting formamidine cation for methylamine cations. Its bandgap width is 1.43 eV, close to the optimal light absorption bandwidth of 1.44 eV. Compared with the methylamine cations, the formamidine ions have a larger ion radius, which will cause the expansion of the lattice, thus affecting the bond length between the halogen ions and the metal ions, and thus changing the perovskite bandgap to be closer to the width of the optimal light absorption forbidden gap.

2.2. Charge transport materials
The charge transport layer consists of two parts: the electron transport material (ETM) and hole transport material (HTM). The ETM plays an important role in electron transporting and hole–electron pair recombination. According to the properties of materials, there are two types of ETM: organic ETM and inorganic ETM. Currently, the most commonly used organic ETM are fullerenes, fullerenes derivatives, nonfullerene and non-fullerene derivative [17–20]. Fullerene conductive materials have matched energy levels that coincide with perovskite light-absorbing materials and electrodes, and their higher electron mobility enables them to have excellent electronic extraction and charge transfer performance, which can effectively inhibit the hysteresis of the *J–V* curve. Both fullerenes and non-fullerenes are widely used in flexible devices due to their low processing temperature. Non-fullerene receptors have more tunable physicochemical properties, more efficient spectral utilization, and a lower energy loss than fullerenes and their derivatives. At present, the PCE of binary system PSCs based on non-fullerene ETL has exceeded 14%, the PCE of the ternary system PSCs has achieved 14.6%, and the PCE of laminated PSCs has also exceeded 17%.

In terms of inorganic ETM, TiO_2 and SnO_2 are the most commonly used materials in PSCs. TiO_2 has a high electron transmission rate, which ensures effective electron injections, and its electrons recombination is slow

and has a high refractive index to light, making it an ideal electron transmission material for PSCs [21, 22]. SnO_2 has a higher mobility than TiO_2, which is also applicable to PSCs [23]. In the existing reports, TiO_2 is generally required to be sintered at high temperature to form an anatase phase for PSCs, while SnO_2 can be prepared at low temperature with a simpler process. Fang *et al* [24, 25] obtained 18% PCE in the low-temperature preparation of SnO_2 plate PSCs, which demonstrates both a higher PCE and stability under light than adopting TiO_2 under the same conditions. In addition to TiO_2 and SnO_2, other inorganic metal oxides such as ZnO_2 and WO_3 are also used as the ETL in PSCs [26, 27].

The HTM plays the multiple role of transmitting holes and blocking electrons, so the energy level of the HTL should match the valence band of perovskite materials, and at the same time, it should have excellent hole transporting ability. HTM is mainly divided into two categories: organic HTM and inorganic HTM. The most commonly used HTM is Spiro-OMeTAD [2]. Jeon *et al* [28] prepared mesoporous perovskite cells (MPSCs) with a PCE of 16.7% by adjusting the sites of methoxy on Spiro-OMeTAD. But Spiro-OMeTAD purification is difficult, and the relatively simple purification process of triphenylamine polymer PTAA has also been applied to PSCs—its related solar cells' PCE is reported to have reached 22.4%. In preparation for spin coating, such triphenylamine polymers are generally doped with Li-TFSI and TBP to improve the hole transporting ability. P3HT has excellent photoelectric performance, is low cost and easy to prepare. At present, the PCE of PSCs achieved 23.3% with P3HT as the HTL [29, 30].

In order to reduce costs, inorganic HTMs with lower preparation costs are often used in PSCs as substitutes. At present, the commonly used inorganic HTMs include CuI, NiO, CuSCN, *et al* [31–33].

2.3. Electrode materials
An ideal electrode requires not only a certain light transmittance, but also a certain energy level, conductivity and roughness. Firstly, the electrode work function should match the ETM. If the difference is large, it is easy to cause a recombination of electrons and holes in the conductive substrate, which affects the performance of solar cells. Better conductivity means a thicker layer of metal oxide, but subsequently

Table 3. Some typical printable small-molecule HTMs for PSCs.

No.	HTM	Highest Occupied Molecular Orbital (HOMO) (eV)	Hole mobility $(cm^2V^{-1}S^{-1})$	Conductivity $(S\,cm^{-1})$	References
1	TTPA-DBQT	4.64	—	4.25×10^{-4}	[37]
2	TTPA-DBST	4.65	—	6.25×10^{-5}	[37]
3	CZ-TA	5.11	1.65×10^{-4}	—	[38]
4	X55	5.23	6.81×10^{-4}	8.43×10^{-4}	[39]
5	X60	—	1.9×10^{-4}	1.1×10^{-4}	[40]
6	X59	5.15	5.5×10^{-5}	1.9×10^{-4}	[41]
7	Bifluo-OMeTAD	5.12	—	—	[42]
8	AH1	5.22	6.49×10^{-4}	1.05×10^{-3}	[43]
9	X21	4.90	—	—	[44]
10	mDPA-DBTP	5.31	6.34×10^{-4}	—	[45]
11	TQ1	5.32	9.45×10^{-5}	6.58×10^{-5}	[46]
12	TQ2	5.30	2.29×10^{-4}	9.19×10^{-4}	[47]
13	Trux-OMeTAD	5.28	2.30×10^{-3}	—	[48]
14	FA-CN	5.30	1.20×10^{-4}	—	[49]
15	V852	—	4.0×10^{-4}	1.60×10^{-5}	[50]
16	V859	—	1.3×10^{-3}	4.20×10^{-5}	[50]
17	V862	—	1.0×10^{-3}	4.90×10^{-5}	[50]
18	FDT	5.16	—	—	[51]
19	TET	5.08	8.2×10^{-4}	—	[52]
20	CzPAF-TPA	5.07	3.13×10^{-4}	—	[53]

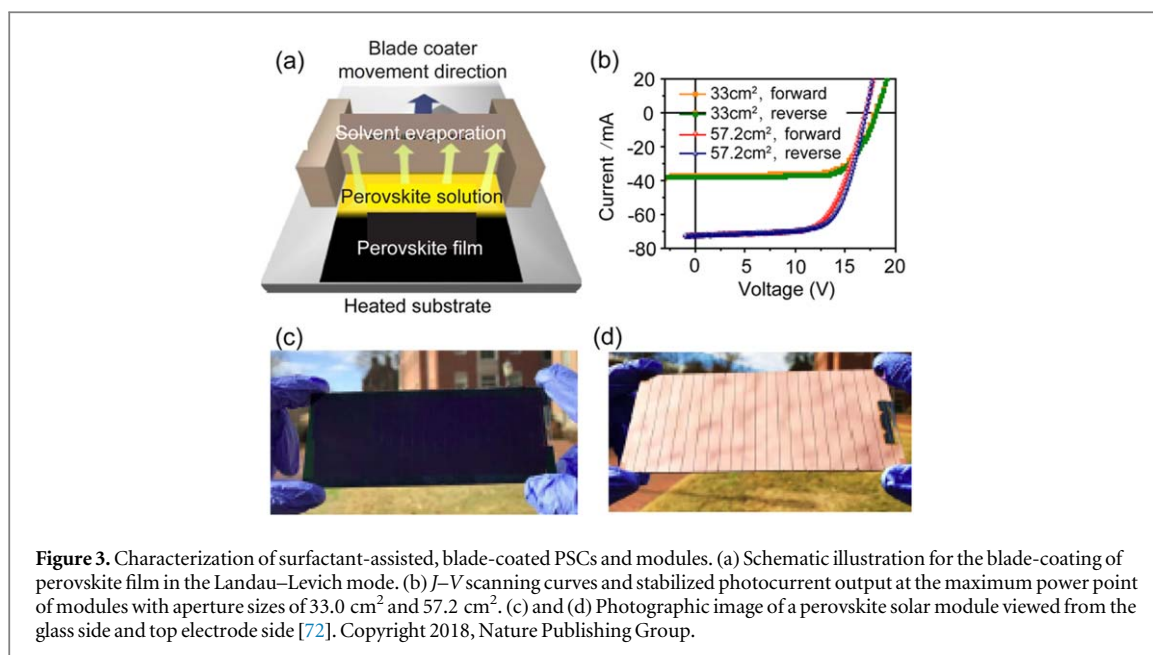**Table 4.** Some typical printable polymeric, organometallic and inorganic HTMs for PSCs.

No.	HTM	HOMO (eV)	Hole mobility $(cm^2V^{-1}S^{-1})$	Conductivity $(S\,cm^{-1})$	References
21	NC-PEDOT:PSS	−5.3	8.3×10^{-5}	—	[54]
22	P3HT/GD	−4.9	1.0×10^{-4}	—	[55]
23	PTAA	−5.2	10^{-3} to 10^{-2}	—	[56]
24	CuPc	−5.2	10^{-3} to 10^{-2}	—	[57]
25	CuPc-OBu	−5.11	4.30×10^{-4}	—	[58]
26	TS-CuPc: F$_4$-TCNQ	−5.3	6.2×10^{-3}	—	[59]
27	HT-ZnPc	−5.19	—	8×10^{-5}	[60]
28	ZnP	−5.29	3.06×10^{-4}	—	[61]
29	NiO$_x$	−5.25	3.75×10^{-3}	—	[62]
30	Cu:NiOx	−5.3	—	1.25×10^{-3}	[63]
31	CuCrO$_2$	−5.4	—	—	[64]
32	CuSCN	−5.3	1.2×10^{-3}	—	[65]
33	ODA-FeS$_2$ NPs	−4.95	3.12×10^{-2}	2.78×10^{-4}	[66]
34	Cu$_{1.75}$S	−5.2	4.47×10^{-3}	5.6×10^{-1}	[67]
35	CuO	−5.4	100	—	[68]
36	CuI	−5.1	9.3	—	[69]

decreases the light transmittance, so materials whose resistance is lower than 15 Ω/sq are commonly used. In PSCs, transparent conductive oxide layers such as ITO or FTO are commonly used as the positive electrode. The work function of both FTO and ITO is about −4.5 eV, which matches the energy levels of TiO$_2$ (−4.0 eV), SnO$_2$ (−4.5 eV), C$_{60}$ (−4.5 V) and other commonly used ETMs. Compared with FTO, industrially-produced ITO has better light transmittance and electrical conductivity, but it is not durable at high temperature. When the temperature is higher than 200 °C, its resistance increased significantly, so it is often used in preparation of the heterojunction structure and flexible device at low temperature. FTO has a higher high-temperature tolerance, which can be

used as the electrode of high-temperature prepared MPSCs, such as TiO$_2$-based MPSCs. For the electrode, metals such as gold or silver etc, which are hot-steamed, are generally adopted [34, 35], and a carbon electrode can also be used [36].

3. Printing inks for PSCs

The core-technology of preparing PSCs through printing is to develop printing inks for suitable industrial printing technologies. Reviewing the development of PSCs, it can be seen that the morphology of thin films and the size of grains are the most important factors. Because perovskite materials are easily affected by water and oxygen in the air, in the preparation process

Figure 3. Characterization of surfactant-assisted, blade-coated PSCs and modules. (a) Schematic illustration for the blade-coating of perovskite film in the Landau–Levich mode. (b) *J–V* scanning curves and stabilized photocurrent output at the maximum power point of modules with aperture sizes of 33.0 cm^2 and 57.2 cm^2. (c) and (d) Photographic image of a perovskite solar module viewed from the glass side and top electrode side [72]. Copyright 2018, Nature Publishing Group.

of PSCs, it is particularly important to improve the stability and condition adaptability of printing ink to obtain continuously uniform thin films without pinholes and appropriate grains size. In this section, the research on printing PSCs ink in recent years is summarized and the properties of perovskite thin films are analyzed.

3.1. Perovskite inks

#### 3.1.1. Strategy of adding ionic liquid additives

Wu *et al* [70] added the ionic liquid additive, methyl ammonium acetate, and the molecular additive, thiocarbamide thiourea (TSC), to the perovskite precursors. The simultaneous use of the two additives improves the fluidity of the perovskite precursor solution and the quality of crystallization, which can be used to prepare large-area and high-quality perovskite film. Based on this, PSCs with an illuminating area of 1.025 cm^2 were prepared through blade-coating. The PCE of PSCs can be maintained above 19% after 1000 h of light illumination. After being stored at 85 °C for 500 h, the printed device can still maintain 85% of its initial PCE. Razza *et al* [71] dissolved the precursor of perovskite in a mixed solvent of N,N-dimethyl formamide, dimethyl sulfoxide (DMSO) and gamma-butyrolactone, and scraped them in air to prepare a PSC device with an area of 10 cm^2 and 100 cm^2, and the PCE achieved 10.4% and 4.3%, respectively. Deng *et al* [72] realized the rapid preparation of large-area, high-quality perovskite thin films by adding surfactant to the precursor ink of perovskite, as shown in figure 3. The study showed that the addition of a small amount of surfactant soy lecithin in the perovskite precursor fluid could form a solvent evaporation flow in the opposite direction of the Marangoni flow, thus realizing the regulation of fluid dynamics and the drying process in the scraping and coating process. In addition, the surfactant can greatly improve the ductility

of ink and improve the quality of large-area films. Based on this ink, the PCE of the PSCs' module with an area of 57 cm^2 achieved 14.6%, and it can continuously work for 20 days without obvious degradation.

Jung *et al* [73] prepared PSCs by adding *N*-cyclohexyl-2-pyrrolidone (CHP) and DMSO into the MAPbI$_3$ solution and combining it with nitrogen-assisted printing with one-step slits coating. The study found that the high boiling point and low vapor pressure of CHP were conducive to the formation of uniform perovskite film, while DMSO could promote grain growth. Based on this ink and full printing method, the PCE of the PSCs module with an area of 35 cm^2 was 12.52%.

Wang *et al* [74] added Cs elements in perovskite precursors, and the flexible, ternary-blended, cationic FA$_{0.945}$MA$_{0.025}$Cs$_{0.03}$Pb(I$_{0.975}$Br$_{0.025}$)$_3$ PSCs were prepared by low-temperature continuous deposition. Experiments show that the addition of Cs elements greatly improves the PSCs' performance and stability. The PCE of flexible PSCs achieved 18.29%, and has an excellent stability and bending resistance. Turren-Cruz *et al* [75] prepared RbCsFAPbI$_3$ perovskite materials by replacing methylammonium molecules with stable formamidinium molecules. Feng *et al* [76] found that dimethyl sulfide additive could effectively improve the film quality of perovskite in a large area. The mechanism is that the lone pair electrons of the S atom in dimethyl sulfide can bond with the vacant orbital of Pb and they interact with each other to form a complex. When the precursor is used to form a film, dimethyl sulfide will slowly dissociate from the complex, thus reducing the growth rate of the perovskite crystal; this is conducive to uniform nucleation and the growth of perovskite crystal, thus improving the quality of large areas of thin film. The PCE of flexible PSCs prepared by dimethyl sulfide additive was significantly increased to 18.4%, as shown in figure 4. In
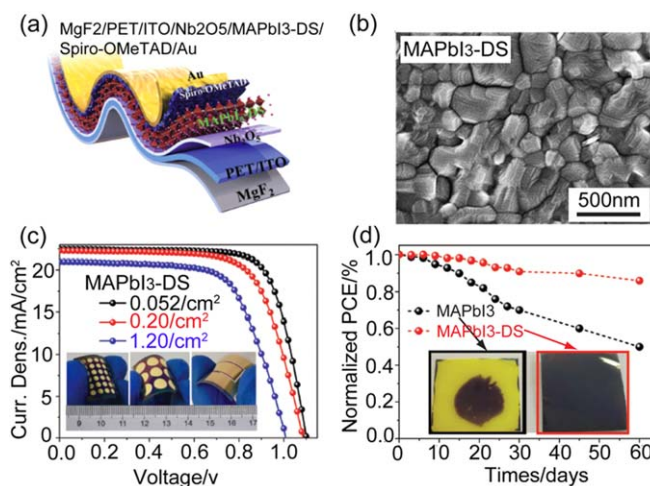
Figure 4. (a) Illustration of the F-PSCs' structure. (b) Top-view scanning electron microscope (SEM) images of MAPbI$_3$-DS films. (c) *J–V* curves of different active areas for the MAPbI$_3$-DS flexible devices. (d) The stability measurements of bare F-PSCs without any encapsulation exposed to ≈35% humidity in a dark condition [76]. Copyright 2018, Wiley-VCH.
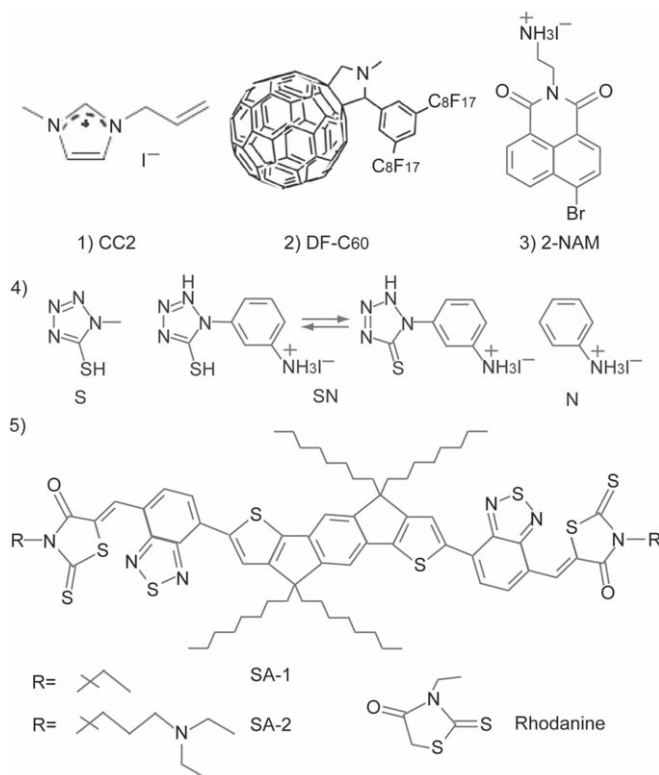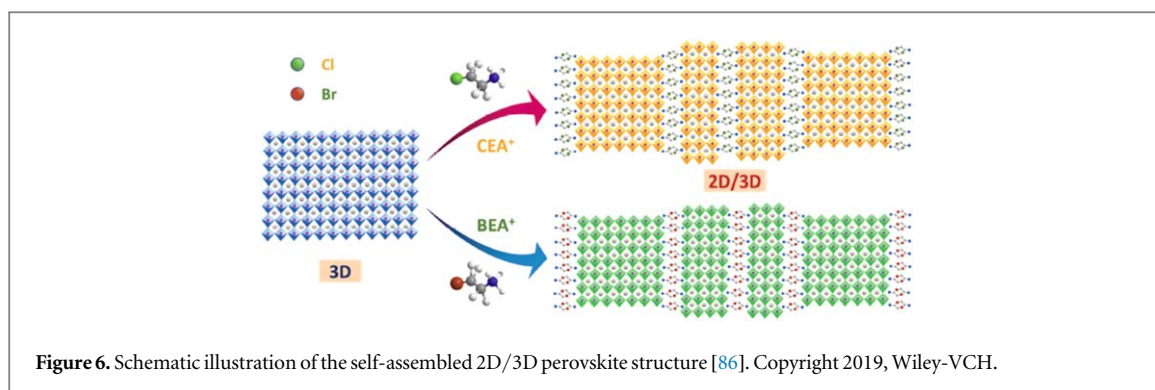

Figure 5. The chemical structure of several ionic additives.

addition, this flexible structure shows good flexural resistance and maintains 86% of its original PCE after 5000 bends at a 4 mm radius of curvature.

Zhang *et al* [77] prepared a perovskite ink with an ionic liquid contained –CH$_2$–CH=CH$_2$ (CC$_2$) functional group (as shown in figure 5(1). Highly uniform perovskite film is prepared using the fumigation method. The results show that CC$_2$ doping can significantly improve film formation quality of perovskite precursor solution. Liu *et al* [78] introduced

two fluorine chains into common fullerenes by substitution, and then added this fluorine-linked fullerene DF-C$_{60}$ (as shown in figure 5(2)) into the perovskite solution to construct perovskite heterostructure materials containing fluoroalkyl-substituted fullerenes. The mixed precursor solution has good film-forming properties. Because two fullerenes with strong hydrophobic fluorine chains are distributed on the upper surface of the perovskite layer (especially at the grain boundary on the upper surface), they effectively block

Figure 6. Schematic illustration of the self-assembled 2D/3D perovskite structure [86]. Copyright 2019, Wiley-VCH.

the moisture in the air from entering the interior of the PSC through the grain boundary, thereby increasing its long-term stability in air. The prepared PSCs maintained 90% of their initial PCE under 60% relative humidity (RH) for 30 days. Wu *et al* [79] added 2-NAM (as shown in figure 5(3)), a new hydrophobic material, into the solution of the precursor of the perovskite material. The results show that 2-NAM is able to combine with perovskite materials through a strong Lewis acid-based interaction, which can effectively increase the size of crystal particles in the perovskite film and reduce the recombination of charge carriers, thus improving the PCE and stability of PSCs. The addition of 2-NAM improves the film formation of ink, which is conducive to the preparation of high-quality perovskite films by continuous printing.
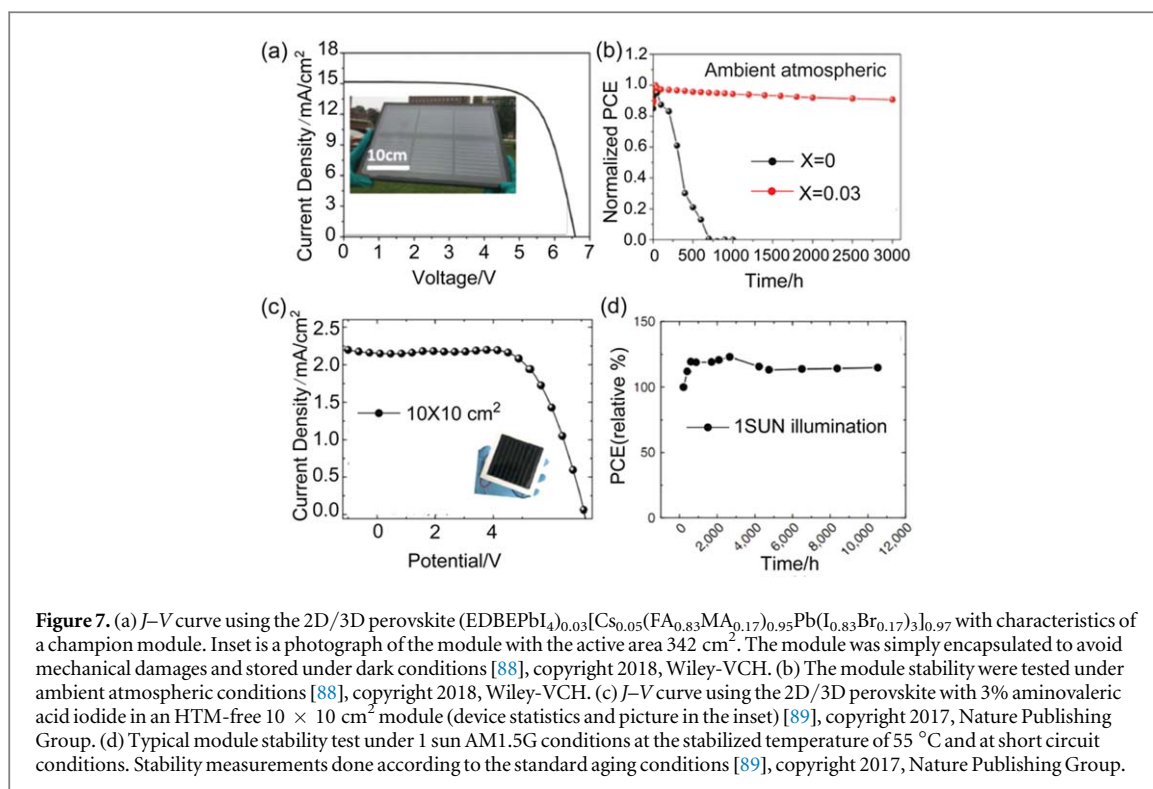
Wei *et al* [80] added polyethylene glycol (PEG), a hydrophobic organic material, and PCBM, a defect inhibiting material, to perovskite precursors. The inks can be used to prepare films at low temperature and have high film-forming properties. The PCBM-PEG-PSC organic conductive network structure prepared with this ink reduces the carrier recombination rate and effectively improves the output stability of the device. Bi *et al* [81] functionalized hydrophobic aromatic groups by introducing mercaptan and amine groups thiol-based 5-(methylthio)-1H-tetrazole (S), ammonium-based anilinium iodide (N), bifunctional 3-(5-mercapto-1H-tetrazol-1-yl) benzenaminium iodide (SN), as shown in figure 5(4), which can inhibit the cation vacancy defect at position A, increase grain size and passivate the surface/interface. Its unique tautomer molecular form can assist crystallization and reduce defects at the same time. This provides a new idea for controlling the crystallization rate of perovskite during printing. The PCE of 1 cm^2 PSCs is more than 20% without the need for a reverse solvent process, which is achievable for large-area devices preparations. Yu *et al* [82] prepared organic conjugated molecules SA-1 and SA-2 with Rhoda nine structures as additives (as shown in figure 5(5)), which not only improves the film formation of perovskite precursor solutions, but also promoted the generation of large-size perovskite grains. The prepared organic-inorganic hybrid PSCs achieved a high PCE of 20.3%, and its long-term stability was significantly improved under high humidity.

3.1.2. Inorganic perovskite materials

Yang *et al* [83] synthesized $CsPb_{1-x}Ge_xI_2Br$ inorganic perovskite precursor ink with good film formation and low preparation temperature. Experiments show that the addition of GeI_2 not only improves the crystal quality of perovskite, but also improves the phase stability of perovskite by inducing lattice strain. Part of Ge^{2+} is oxidized into Ge^{4+} in the air and passivates the perovskite surface, which is conducive to improving the environmental fitness of the printed perovskite film and the corresponding flat-plate PSCs can achieve a stable PCE of 10.8% in 50%–60% high humidity air. Liang *et al* [84] synthesized an inorganic perovskite material $CsPb_{0.9}Sn_{0.1}IBr_2$ with mixed Pb^{2+}/Sn^{2+} and mixed I^-/Br^-. This inorganic perovskite has good solubility and easily forms film. It is very convenient to prepare perovskite thin film with this material, which does not need to be operated in a glove box. The stability of the device has been greatly increased. Therefore, it is suitable for large-area printing process. The encapsulated devices demonstrated nearly no reduction after three months at an ambient condition and some devices survived for more than two weeks at 100 °C. Xiang *et al* [85] synthesized a new $CsPb_{0.95}Eu_{0.05}I_2Br$ all-inorganic perovskite ink using europium doping. The doping of europium greatly improves the film-forming quality of inorganic perovskite precursors, while the crystal properties can be regulated. The obtained all-inorganic perovskite films have no holes, which provides a new idea for the preparation of large-area printed perovskite inks. Perovskite films prepared based on this material can be stable for more than six months under a condition of less than 40% RH. The PCE of inorganic PSCs achieved 13.71% and shows good stability under continuous one sun illuminating.

3.1.3. Multidimensional perovskite mixture

Liu *et al* [86] prepared a two-dimensional/three-dimensional (2D/3D) perovskite precursor ink by introducing 2-chloroethylamine hydrochloride (CEA) and 2-bromoethylamine hydrobromide (BEA) into a cesium/methimazole-mixed cationic 3D perovskite precursor (as shown in figure 6). This 2D/3D perovskite precursor ink has high film-forming properties and high crystallinity. The formed film is flat and dense, which is very suitable for the large-area

Figure 7. (a) *J–V* curve using the 2D/3D perovskite (EDBEPbI$_4$)$_{0.03}$[Cs$_{0.05}$(FA$_{0.83}$MA$_{0.17}$)$_{0.95}$Pb(I$_{0.83}$Br$_{0.17}$)$_3$]$_{0.97}$ with characteristics of a champion module. Inset is a photograph of the module with the active area 342 cm^2. The module was simply encapsulated to avoid mechanical damages and stored under dark conditions [88], copyright 2018, Wiley-VCH. (b) The module stability were tested under ambient atmospheric conditions [88], copyright 2018, Wiley-VCH. (c) *J–V* curve using the 2D/3D perovskite with 3% aminovaleric acid iodide in an HTM-free 10 × 10 cm^2 module (device statistics and picture in the inset) [89], copyright 2017, Nature Publishing Group. (d) Typical module stability test under 1 sun AM1.5G conditions at the stabilized temperature of 55 °C and at short circuit conditions. Stability measurements done according to the standard aging conditions [89], copyright 2017, Nature Publishing Group.

continuous printing process. When 5% CEA was introduced, the highest PCE was 20.08%. The device maintained 92% of its initial PCE after aging at 50 ± 5% RH for 2400 h.

Ye *et al* [87] introduced amphoteric molecule 5-ammoniumvaleric acid (5-AVA) into the perovskite light-absorbing material MAPbI$_3$, and obtained 2D/3D perovskite material (AVA)$_2$PbI$_4$@MAPbI$_3$. The PSCs of a mesoporous structure without a HTL were prepared by screen printing. The PCE of PSCs achieved 18.0%, maintaining 90% of its initial PCE for 32 days under inert conditions and 72% of its initial PCE for 20 days under normal air conditions. Li *et al* [88] introduced 2D perovskite material (EDBEPbI$_4$)$_{0.03}$(MAPbI$_3$)$_{0.97}$ into the precursor of 3D perovskite Cs$_{0.05}$(FA$_{0.83}$MA$_{0.17}$)$_{0.95}$Pb(I$_{0.83}$Br$_{0.17}$)$_3$ and obtained 2D/3D perovskite material (EDBEPbI$_4$)$_{0.03}$[Cs$_{0.05}$(FA$_{0.83}$MA$_{0.17}$)$_{0.95}$Pb(I$_{0.83}$Br$_{0.17}$)$_3$]$_{0.97}$. The PSCs were prepared by the full printing method and the PCE achieved 21.06%. The initial PCE could be maintained at 90% after 3000 h in air, as shown in figures 7(a) and (b). Grancini *et al* [89] made a carbon-based MPSCs module with an area of 10 × 10 cm^2 using the full printing method based on [HOOC(CH$_2$)$_4$NH$_3$]$_2$PbI$_4$/CH$_3$NH$_3$PbI$_3$. The PCE of PSCs achieved 11.2%. After being illuminated under 1 sun sunlight and 50 °C for 10 000 h, the PCE has almost no losses, as shown in figures 7(c) and (d).

3.1.4. Green solvent materials
The best choice is to prepare perovskite film by the solvent method. However, almost all the solvents used in highly efficient PSCs are chlorobenzene (CB), toluene, etc. These solvents are toxic, environmentally

unfriendly, and not suitable for large-scale production. Yavari *et al* [90] used anisole (ANS) as a solvent to prepare PSCs in and out of the glove box, respectively achieving a PCE of 19.9% and 15.5%. Bu *et al* [91] used the benign solvent ethyl acetate (EA) to replace the counter solvent in the preparation process of PSCs and the highly toxic and carcinogenic solvent CB commonly used to dissolve Spiro-OMeTAD, the ETM, which not only improved the quality of the perovskite film, but also significantly improved the PCE of PSCs. Among them, the PCE of small area PSCs achieved 19.43% (0.16 cm^2 illumination aperture area), and the PCE of the small component achieved 14.28% (5 × 5 cm^2), as shown in figure 8. The use of green solvent engineering is also suitable for printing large areas of non-pinhole perovskite film and PSCs components. The increase of the perovskite performance is mainly due to the increase of charge transfer and decrease of interfacial recombination after solvent treatment.

3.2. Printable electrons transport layer materials
Printable electrons transfer materials need to be not only stable and inexpensive, but also, more importantly, have high dispersion, easy film formation, and be low-temperature processable. At the same time, they need to have an electrons transfer layer ink with a stable environment and work functions matching with the metal electrode. This will greatly simplify the manufacturing of PSCs. More importantly, the characteristics of low-temperature preparation make it more compatible with flexible electronic devices,
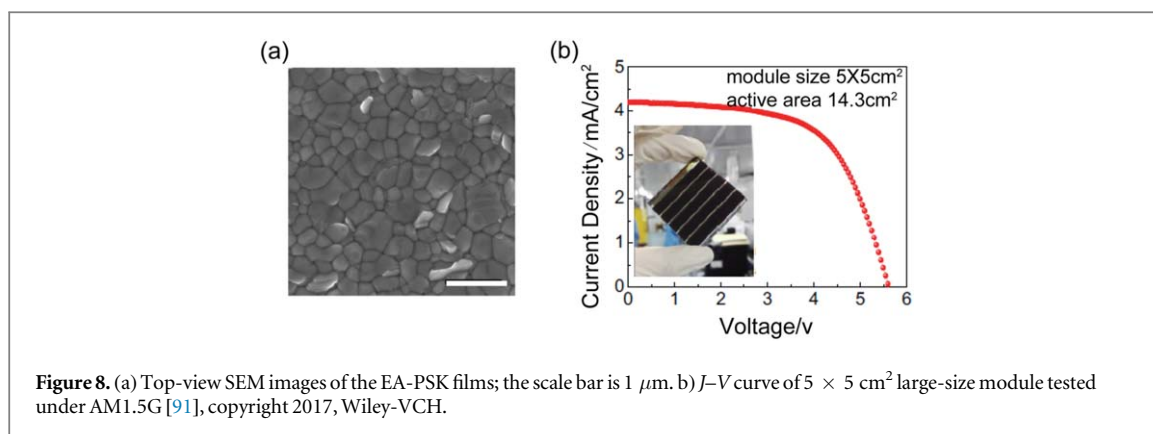
Figure 8. (a) Top-view SEM images of the EA-PSK films; the scale bar is 1 μm. b) *J–V* curve of 5 × 5 cm² large-size module tested under AM1.5G [91], copyright 2017, Wiley-VCH.
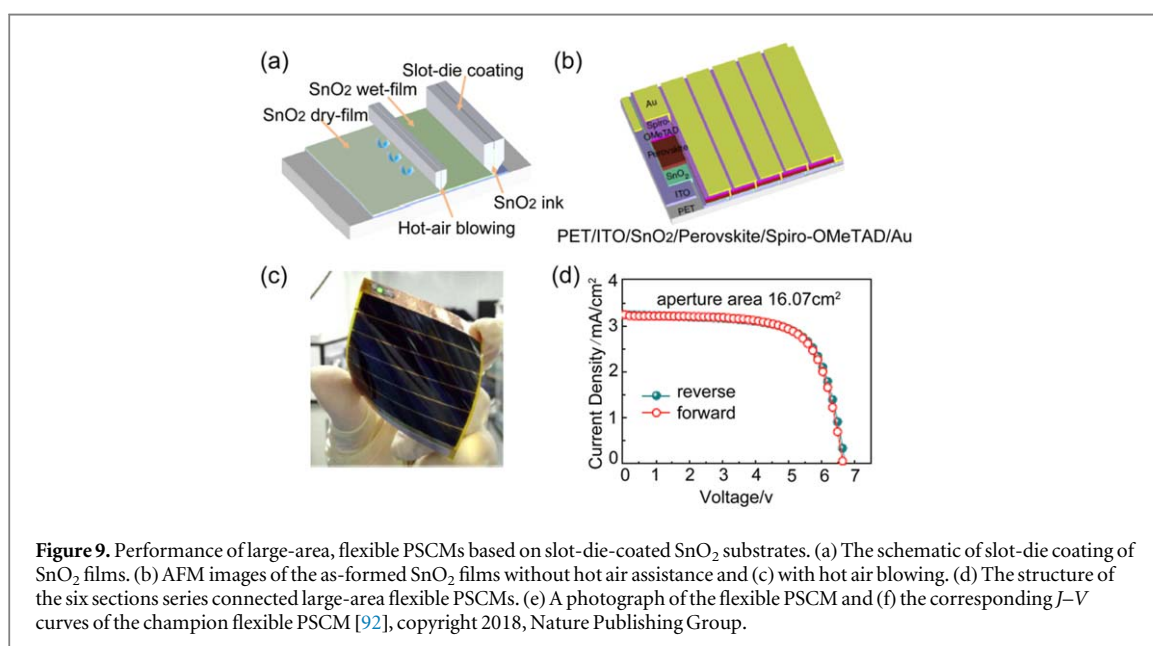

Figure 9. Performance of large-area, flexible PSCMs based on slot-die-coated SnO₂ substrates. (a) The schematic of slot-die coating of SnO₂ films. (b) AFM images of the as-formed SnO₂ films without hot air assistance and (c) with hot air blowing. (d) The structure of the six sections series connected large-area flexible PSCMs. (e) A photograph of the flexible PSCM and (f) the corresponding *J–V* curves of the champion flexible PSCM [92], copyright 2018, Nature Publishing Group.

which is also a necessary condition for printing wearable products. Therefore, developing new electronic transmission materials suitable for printing and forming is a key research direction.

Commercial SnO₂ printing inks can cause etching of the printing die and fail to produce a large area of smooth SnO₂ interfacial layer. Bu *et al* [92] solved this problem by doping KOH into commercial SnO₂ printing ink. KOH doping can effectively adjust the acidity and alkalinity of ink to meet the needs of protecting the printing die head. In addition, K⁺ can promote the crystal nucleus growth of perovskite in the SnO₂ interfacial layer to prepare high-quality perovskite thin films, and K⁺ can fill the crystal vacancy of perovskite and be passivated in the interface layer. Through the application of this strategy, large-area, high-quality SnO₂ thin films were prepared through slit extrusion printing. In the interface layer of SnO₂, 16.07 cm² non-hysteresis flexible PSC modules were prepared, and the PCE exceeds 15%, as shown in figure 9. Chen *et al* [32] prepared a Ti(Nb)O$_x$ heavily doped charge transfer layer material. The material has good solubility and good film formation (as shown in

figure 10(1)). Ti(Nb)O$_x$ films prepared have no defects in a large area and have high efficiency in the extraction and separation of photon-generated charges. Under the condition of increasing the working area of the PSCs by about ten times, the PCE of large-area PSCs achieved 15% (1 cm² illumination aperture area). Wei *et al* [93] prepared ZnO nano-materials modified by a silane coupling agent. The ink can be stored in the atmosphere for at least a year, and the nanoparticles do not show significant aggregation. Using ink stored for one year to prepare the interface material, excellent device performance can also be obtained, which provides a new idea for developing high-stability printable nano-materials ink.

Song *et al* [94] deposited 0.08 wt% polyallyl amine (PAA) solution on the surface of fullerene C₆₀ and it reacted for 60 s at 150 °C, finally synthesizing an insoluble and stable C₆₀-PAA ETM. This study provides a new method to improve the performance of large-area printed C₆₀ film. Li *et al* [95] used the new fullerene-pyrrole derivative C₆₀-N (as shown in figure 10(2)) to replace PCBM as the ETM. The C₆₀-N has good film-forming properties and is suitable for printing

Figure 10. Chemical structures of printable ETMs for solar cells.
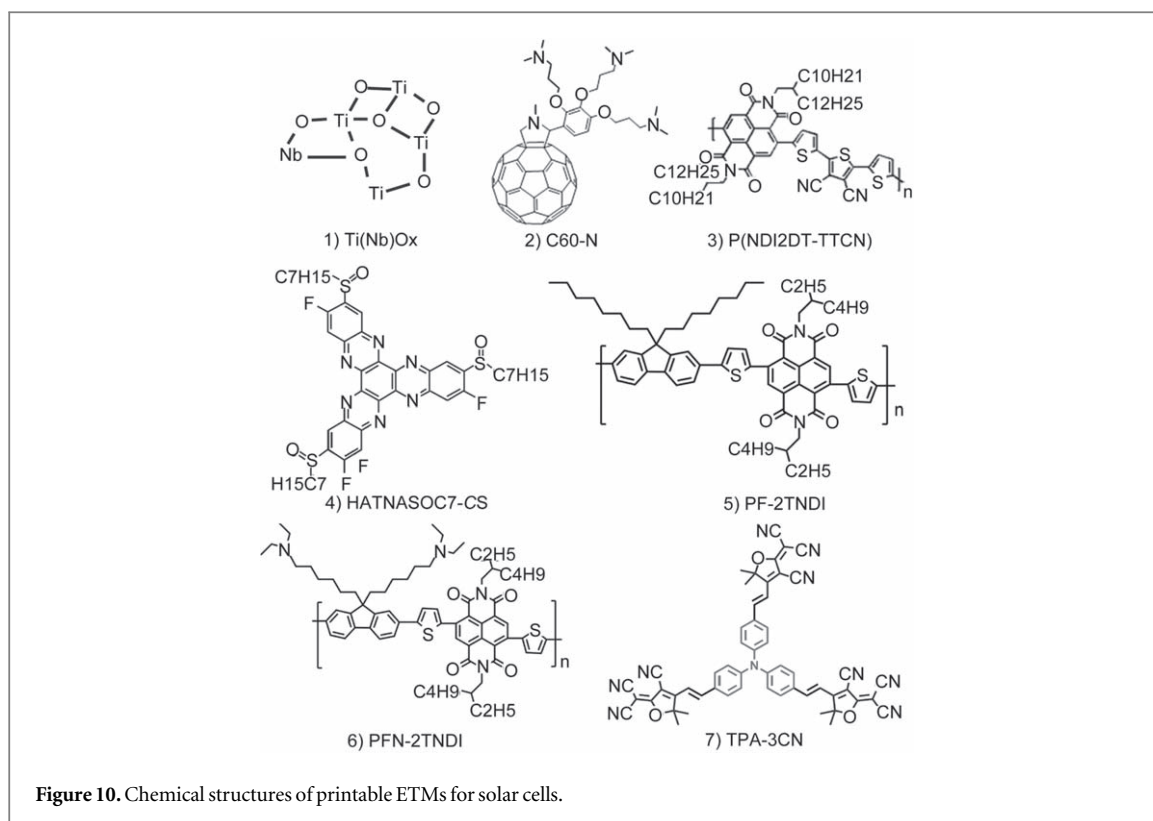
processes. By using C_{60}-N as the ETL, the PCE of PSCs achieved 16.6%, while the PCE of PSCs based on PCBM is only 12.3%. This is because C_{60}-n can significantly change the work function of metal electrodes. At the same time, as the electron-rich groups of C_{60}-N can passivate surfaces of perovskite materials. The defect states on surfaces are reduced, so the PCE is improved and demonstrates a better repeatability.

Kim *et al* [96] designed and synthesized a novel polymer P(NDI2DT-TTCN) containing naphthalimide (as shown in figure 10(3)) to replace fullerenes as ETM. Compared with the fullerene-type ETL, the ETL prepared by P(NDI2DT-TTCN) not only has a better solubility and film formation, but also improves electron transport capacity and stability. After 500 bending cycles, micro-cracks and layer separation occur between PCBM and perovskite, and the PCE can only remain at 13%. However, the PCE of the P(NDI_2DT-TTCN) device maintains 74% of its initial PCE. Zhao *et al* [97] developed a series of novel HATNA derivatives and regulated their dispersity by introducing different numbers of fluorine atoms, sulfoxides or sulfones into HATNA molecules. Among them, HATNASOC7-Cs (as shown in figure 10(4)) has the best dispersibility, and the PCE of PSCs achieved 17.6% with HATNASOC7-Cs as an ETL.

Sun *et al* [98] prepared a new type of N-type conjugated polymer material PF-2TNDI and PFN-2TNDI (as shown in figure 10(5 and 6)), which was applied in PSCs and achieved a PCE of 16.7%. At the same time, the device performance of the polymer on the dependence of the ETL thickness is low. When its thickness increases to 200 nm, the device PCE can still be maintained at more than 14%, which is beneficial for the large-area technology production of coil-to-coil in the future, and provides a possibility for the large-area printing of perovskite thin film solar cells in coil-to-coil. Chen *et al* [99] synthesized a novel D-A non-fullerene ETM TPA-3CN by molecular engineering methods for small-molecule materials with triphenylamine (TPA) as the donor and (3-cyano-4,5, 5-trimethyl-2 (5 H) -furanolide) malononitrile (3CN) as the receptor, as shown in figure 10(7). Based on TPA-3CN's low-temperature performance and good film-forming ability, the flexible inverted-phase PSCs were prepared, and the PCE achieved 13.2%.

Wang *et al* [100] developed nano-composite interface materials MoO_3: PEDOT: PSS based on metal oxide nanoparticles and polymers. The MoO_3: PEDOT: PSS has excellent film-forming properties and photoelectric properties. Composite metal oxide nano-material with polymers not only avoided the agglomeration of metal oxide nano-materials, but also the restriction of film thickness in polymer materials due to conductivity. The MoO_3: PEDOT:PSS which was used in PSCs can reduce the dependence between the solar cells' performance and interfacial thickness, which will improve the printability repeatability and solar cells' yield.
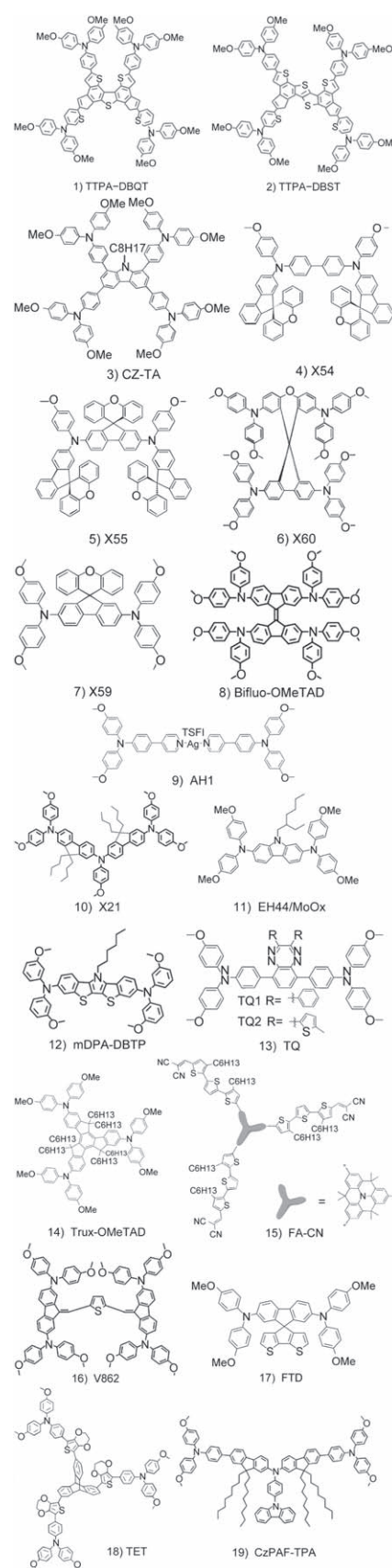
3.3. Printable HTMs

For inks used for printing a HTL, it is not only required that the HTL has high thermal stability, high hole mobility, is precisely matched with the perovskite energy level, has photochemical stability and low costs, but also has good dispersibility and film formation.

3.3.1. Organic small-molecule HTMs

Javier *et al* [37] reported on the synthesis and characterization of two novel small-molecule HTMs for PSCs. The new compound was based on DBQT and DBST, two kinds of heterocyclic thiophene 'core', and was covalently linked with triphenylamine groups to obtain the four-arm tetraphenyl-triamine (TTPA) derivatives TTPA-DBQT and TTPA-DBST (as shown in figure 11(1 and 2)). The material is soluble, film forming, and has good electronic contact with perovskite, which can effectively extract holes. The PCE of the PSCs achieved 18.08% with TTPA-DBQT as the HTL. Yin *et al* [38] obtained a HTM CZ-TA which has good film-forming ability (as shown in figure 11(3)). The PCE of the PSCs based on CZ-TA was 18.32% with a filling factor up to 81%, and its synthesis cost is only 1/20 of Spiro-OMeTAD.

Xu *et al* [39, 40] synthesized organic small-molecule HTMs, X54, X55 and X60 (as shown in figure 11(4, 5, 6)) by designing Snail [Fluorene-9, 9-Xanthene] (SFX). The PSCs prepared with X55 and X60 obtained 20.8% and 19.84% PCE respectively. Under the same conditions, its photoelectric performance was much higher than that of Spiro-OMeTAD (18.8%). Importantly, this kind of organic small-molecule HTM has good film forming, high solubility, low cost, and does not need the purification process, which brings hope for the future industrial development of PSCs. Bi *et al* [41] optimized the X59 compound with a helical structure (as shown in figure 11(7)), which has high solubility and good film forming. The PCE of PSCs achieved 19.8% with X59 as the HTL under dark and dry conditions. Moreover, the hysteresis of the PSCs was significantly reduced, and the PCE of the device remained at the initial 97.5% after being placed in dark and dry conditions for five weeks, with good repeatability.

Qin *et al* [42] synthesized Bifluo-OMeTAD as a HTM by molecular design (as shown in figure 11(8)). The chemical structure of the material can effectively control the crystallization rate of the film during the printing process and has a good film-forming property. Finally, the open circuit voltage of PSCs prepared by the slit coating method achieved 1.1 V, and the PCE achieved 14.75%. Sun *et al* [43] prepared AH1 (as shown in figure 11(9)) as a HTM and the PCE of the PSCs achieved 11.98% with AH1 as the HTL. Although AH1 has no great advantage over Spiro-OMeTAD in terms of PCE, AH1 has obvious advantages over Spiro-OMeTAD in film-forming ability, and thus has more potential in printing preparation. Zhang *et al* [44] prepared a series of star-shaped small molecular structures by a simple synthesis method. The series of materials have a good film forming, strong hygroscopicity, and their energy levels match

Figure 11. Chemical structures of printable small-molecule HTMs.

well with perovskite materials, and the hole mobility is also very high. Among them, the PCE of PSCs achieved 17.33% with X21 (figure 11(10)) as the HTL.

Christians *et al* [45] prepared a novel composite HTM EH44/MoO$_x$ (figure 11(11)) as an alternative to Spiro-OMeTAD, which can be formed at low temperature and has good dispersion. The HTL prepared based on this material can be in close contact with perovskite film and is very dense, which was very beneficial in improving the stability and PCE of the PSCs. Under the simulated lighting condition with the maximum power density, the unpackaged devices can still maintain 94% of their initial PCE after 1000 h.

Azmi *et al* [46] synthesized the undoped small-molecule HTM mDPA-DBTP with bis (1-benzothiophene)-[3,2-b:2′,3′-d] pyrrole as the core design, as shown in figure 11(12). Compared with the Spiro-OMeTAD doped material, this material has high dispersibility and good film forming; when used as a HTL the PCE of PSCs reaches 18.09%. In addition, due to the hydrophobicity of this small molecule, PSCs have good air stability and can maintain 81% of the initial PCE after 33 days in the air, which is of great significance for large-scale PSC device production.

Zhang *et al* [47] constructed a new HTM (TQ1 and TQ2, figure 11(13)) with the structural characteristics of donor-acceptor-donor (D-A-D) by taking a weak electron-absorbing quinoxoline unit as the core and introducing a methoxyl-substituted triphenylamine unit on both sides through a simple Suzuki coupling reaction. Compared with the electron-rich π bridging, the introduction of a weak absorption electron unit improves the crystallization stability of materials in solution engineering, which easily forms uniform films with stable morphology. The PCE of large-area PSCs (1.02 cm^2) achieved 18.50% with TQ2 as the HTL, which was mainly due to the excellent film-forming property of TQ2. Huang *et al* [48] synthesized the compound Trux-OMeTAD by using three symmetrical aryl amine-containing terminals and truxene with ethyl side chains (as shown in figure 11(14)). The compound has good solubility and film-forming properties, and has a good planar rigid structure. The PCE of PSCs achieved 18.6% with Trux-OMeTAD as the HTL, without obvious hysteresis.

Paek *et al* [49] prepared a star-type D-π-A-type molecule FA-CN which has high dispersibility and good film forming (as shown in figure 11(15)). The PCE of the PSCs achieved 18.9% based on the non-doped FA-CN HTL and mixed perovskite (FAPbI$_3$)$_{0.85}$(MAPbBr$_3$)$_{0.15}$. The maximum power output (MPO) value of its unencapsulated PSCs can still maintain 65% of the initial PCE after 1300 h, which is much higher than the 15% based on Spiro-OMeTAD. Malinauskas *et al* [50] used cheap diphenylamine to replace the fluorene small-molecule V862 (figure 11(16)) as the HTM, and the PCE of PSCs achieved 19.96% with V862 as the HTL. This is mainly due to the excellent film-forming property of V862.

Saliba *et al* [51] synthesized a novel HTM FDT by molecular engineering technology which has good film forming (as shown in figure 11(17)). The PCE of the PSCs achieved 20.2% based on FDT HTL and mixed perovskite(FAPbI$_3$)$_{0.85}$(MABrI$_3$)$_{0.15}$, far higher than that of the PSCs prepared by Spiro-OMeTAD in the same condition. Moreover, FDT is a relatively cheap material, which meets the needs of the commercial development of PSCs.

Sun *et al* [52] synthesized a kind of efficient HTM TET by efficient Stille coupling with a new triptycene as the core and EDOT to regulate the energy level (as shown in figure 11(18)). The TET has excellent solubility, so toluene and other non-halogen solvents can be used in the preparation of solar cells. At the same time, the low price of the material is suitable for application-oriented printing production. Reddy *et al* [53] designed and synthesized a new HTM CzPAF-TPA (as shown in figure 11(19)), and successfully applied it to flip plane heterojunction PSCs and bulk heterojunction flip organic solar cells, both of which can obtain high PCE and stable rigid and flexible devices, providing a new material for the flexible printing cavitation layer.

Gao *et al* [101] prepared a conjugated compound material 6T-p-DP with a 3D dendritic structure. The 6T-p-DPP has stronger single-walled carbon nanotube (SWCNT) dispersion than linear compounds and excellent charge transport performance, good solution process ability and high flexibility. A carbon nanotube thin film transistor was prepared by a printing method using semiconducting SWCNT (s-SWCNT)@6T-p-DPP ink, and the hole mobility achieved 56.6 cm^2 V^{-1} s^{-1}. Some typical printable small-molecule HTMs for PSCs and their properties are listed in table 3.

3.3.2. Polymer HTMs

Poly(3,4-ethylenedioxythiophene): poly (styrenesulfonate), PEDOT: PSS (as shown in figure 12(20)) is an important p-type organic semiconductor, which can be prepared at low temperature and has good adaptability with a flexible substrate. Hu *et al* [54] introduced a NaCl doped PEDOT: PSS, which not only improved its electrical conductivity, but also improved the quality of the upper perovskite film through the small NaCl crystals distributed on the surface. PSCs prepared in this simple way also increase the filling factor and open circuit voltage, which improves the PCE of PSCs from 15.1% on average to 17.1% and 18.2% at the highest, with little hysteresis. This strategy is greatly compatible with printing technology, so as to achieve high PCE and realize the mass production of PSCs with adjustable crystal orientation.

Poly(3-hexylthiophene) (P3HT) (as shown in figure 12(21)) is an electron donor material in organic solar cells and an ideal p-type semiconductor with good hole mobility. It can also be used as a HTM in organic and inorganic hybrid PSCs [102]. Xiao *et al* [55] doped graphene into P3HT as a HTM. Measurements by Raman spectroscopy and ultraviolet photoelectron
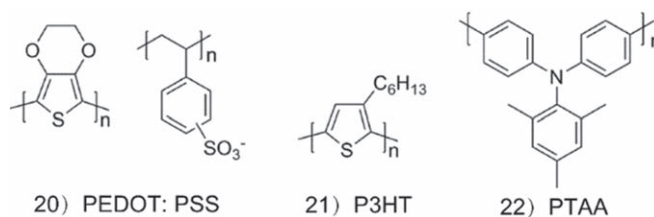
Figure 12. Traditional commercial polymeric HTMs for PSCs.
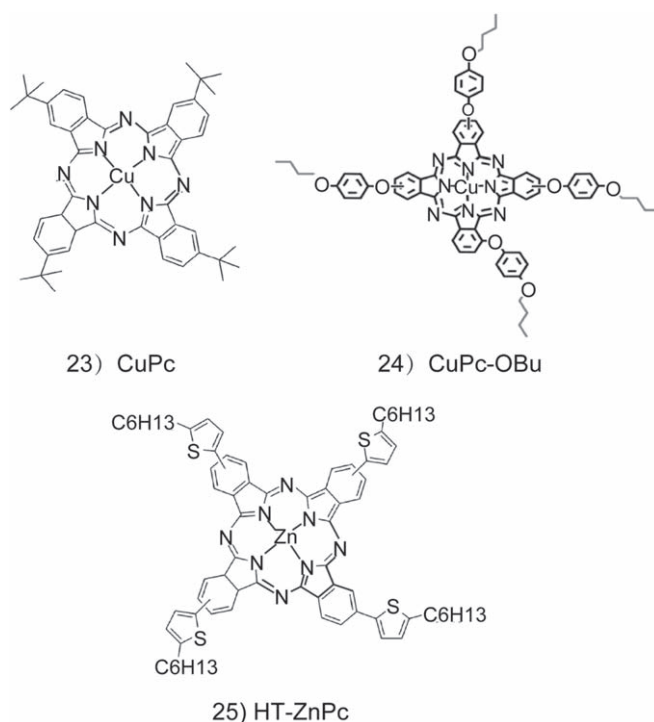
Figure 13. Printable organometallic HTMs for PSCs.

spectroscopy revealed a strong π-π bond between graphene and P3HT, improving the quality of the film forming of P3HT and solar cells' performance. The PCE of the prepared PSCs achieved 14.58%.

Poly-[bis(4-phenyl)(2,4,6-trimethylphenyl)amine] (PTAA) (as shown in figure 12(22)) was used in PSCs due to its excellent hole mobility, 1×10^{-2} to 1×10^{-3} cm^2 V^{-1}s^{-1}. Currently, the PCE of PSCs with PTAA as the HTL exceeds 22% [56]. However, PTAA is very expensive (about $2000 g^{-1}), so it is not feasible for industrial production. However, polymer ETMs containing such aniline structures have better film-forming properties and higher hole mobility than organic small-molecule HTMs, thus revealing great potential for development.

3.3.3. Organometallic HTMs

Zhang *et al* [57] synthesized highly dispersive copper phthalocyanine CuPc nano-rods (as shown in figure 13(23)) to replace Spiro-OMeTeD. At the same time, a commercial carbon pair replaced Au as the electrode pair for PSCs. It was found that the application of a copper phthalocyanine nanorod effectively

promoted charge separation and inhibited electron recombination. After optimization, the PCE of PSCs achieved 16.1%, and the PCE remained at the initial 91.3% after being placed in an ambient atmosphere at room temperature without encapsulation for over 500 h under one sun illumination. Jiang *et al* [58] synthesized a new copper phthalocyanine derivative CuPc-OBu (as shown in figure 13(24)), which has good solubility and stable crystallization. The PCE of non-doped CuPc-OBu PSCs achieved 17.6%. Wang *et al* [59] prepared the mixed HTL by doping the solution with TS-CuPc with good solubility and F$_4$-TCNQ with strong electronic affinity. The TS-CuPc film treated with p-type doped solution can effectively improve the conductivity and hole mobility of the film. In addition, almost neutral TS-CuPc was obtained through doping. In contrast to the acidity of PEDOT: PSS, neutral TS-CuPc avoids electrode corrosion and is conducive to improving device stability. Finally, the PCE of the p-i-n structure achieved 16.14%. The developed TS-CuPc: F$_4$-TCNQ provides a variety of HTM in the plane PSCs. In addition, the

solubility of the main material TS-CuPc in water is relatively high, which makes the preparation of TS-CuPc aqueous solution quite simple, eco-friendly and non-toxic. The process of F_4-TCNQ doped TS-CuPc can be achieved by mixing TS-CuPc and F_4-TCNQ solution based on low-temperature solution, without needing an additional oxidation process.

Cho *et al* [60] reported on a series of HTMs after modification of phthalocyanine zinc groups, respectively modifying tert-butyl, thiophen-hexyl and thiophen-hexyl ht-znpc on the periphery (as shown in figure 13(25)). The HT-ZnPc has good solubility and a low preparation temperature. The PCE of PSCs achieved 17.5% based on a HT-ZnPc HTL and mixed perovskite $(FAPbI_3)_{0.85}(MAPbBr_3)_{0.15}$. Chen *et al* [61] reported on a HTM based on a porphyrin group complexation of zinc and copper. When ZnP of a zinc atom is applied to PSCs, 17.78% PCE can be obtained. When ZnP-based PSCs are at room temperature and 40%-50% HR, their PCE can still maintain at an initial 90% after a month, while PSCs based on Spiro-OMeTAD can only maintain about 45% of the initial PCE.

3.3.4. Inorganic HTMs

Yin *et al* [62] prepared a highly dispersed solution of NiO_x nanoparticles. The solution has good film-forming properties and can be formed at a low temperature of 130 °C. Jung *et al* [63] doped Cu into NiO_x to form $Cu:NiO_x$ and used it as a HTM. The doping of Cu improves the surface roughness of NiO_x film and improves its wettability, so as to improve the film formation of the next layer of solution, which is conducive to printing perovskite layers.

Zhang *et al* [64] prepared $CuCrO_2$ solution that can be shaped at low temperature and better solubility. In addition, they found that the $CuCrO_2$ layer has stronger UV light absorption ability, which can effectively prevent the destruction of the perovskite layer by UV light, so that the light stability of the device can be greatly improved.

Yang *et al* [103] modified CuSCN and obtained CuSCN solution with high dispersion and no dopants, and prepared dense CuSCN film by spraying at 80 °C at low temperature. The PCE of PSCs prepared by this method achieved 17.1%. Arora *et al* [65] dissolved CuSCN salt in diethyl sulfide to form CuSCN solution. This strategy improves the film-forming quality of CuSCN. The short current density of PSCs prepared by this method achieved $23.4\ mA\ cm^{-2}$, and the PCE achieved 20.3%. The PCE of the PSCs remained at the initial 88% after being placed in a dark place under 85 °C for 1000 h, showing that the material has good stability.

Koo *et al* [66] prepared the highly dispersive octade-cylamine-capped pyrite nanoparticles(HTM ODA-FeS_2 NPs) and applied them to PSCs, obtaining 12.56% PCE. The PCE remained stable for 1000 h after the PSCs were placed at 50% RH. Lei *et al* [67] introduced a layer of inorganic p-type HTM copper sulfide (Cu_xS, $x = 1.75$) on the surface of spiro film by the vacuum thermal evaporation method, and prepared a high-quality HTL and

a high-performance perovskite PSC device. Cu_xS thin film can be deposited at room temperature without post-annealing and has high hole mobility ($4.47\ cm^2\ V^{-1}\ s^{-1}$), which improves the hole mobility of the device. More importantly, Cu_xS is flat and compact; it can fill holes on the surface of the spiro film caused by Li ion migration, and has excellent hydrophobicity (water contact angle 91.64°). This means that it can resist moisture erosion in the air, which greatly improves the stability of PSCs in moist air. The PCE of Cu_xS-based PSCs achieved 18.58% and remained at more than 90% of their initial PCE after being stored at 40% HR for 1000 h. Some typical printable polymeric, organometallic and inorganic HTMs for PSCs and their properties are listed in table 4.

3.4. Printable electrode materials

3.4.1. Printable bottom electrodes materials

Li *et al* [104] synthesized silver nanowires (AgNWs) with a diameter of 20 nm and a length-to-diameter ratio of 2000. By coating printing, they are prepared into flexible transparent conductive film; the light transmittance was 99.1%, the resistance is 130.0 Ω/sq. Li *et al* [105] prepared a kind of conducting polymer by using an embedded silver grid and (PH1000) flexible composite electrode (as shown in figure 14(A)), with about 3 Ω/sq low surface resistance; within the scope of visible light, transmittance can reach 82%–86%. The PSCs prepared with this electrode obtained 14% PCE. After more than 5000 full bends, the PSCs remained at more than 95% PCE. The research results provide a possibility for further promoting the application of flexible PSCs in wearable energy. Xiong *et al* [106] designed and prepared a stable, flexible, transparent electrode with high transparency and a low resistance silver nanowire@ionic liquid gel composite. When the electrodes maintain 86% of visible light transmittance, the resistance is 8.4 Ω/sq. Moreover, the performance of the composite transparent electrode remained basically unchanged after being exposed to air for two months, and it was able to endure the acid and alkali treatment required in the photolithography process, which was beneficial to the subsequent patterned processing. This silver nanowire@ionic liquid gel composite provides a new design idea for the preparation of high-performance, flexible, transparent electrodes.

Wu *et al* [107] prepared gold, silver and copper grid electrodes respectively (as shown in figure 14(B)). These electrodes provide excellent electrical conductivity with a high degree of transparency, and the material can be easily transferred to a variety of other substrates while remaining flexible. The research shows that although the electrical conductivity of the copper nano-grid is better, the stability of the gold is the best. Jeon *et al* [108] used HNO_3-treated SWCNTs (HNO_3-SWCNTs) to replace ITO. The PCE of the prepared, flexible PSCs achieved 5.38% (figure 14(C)).
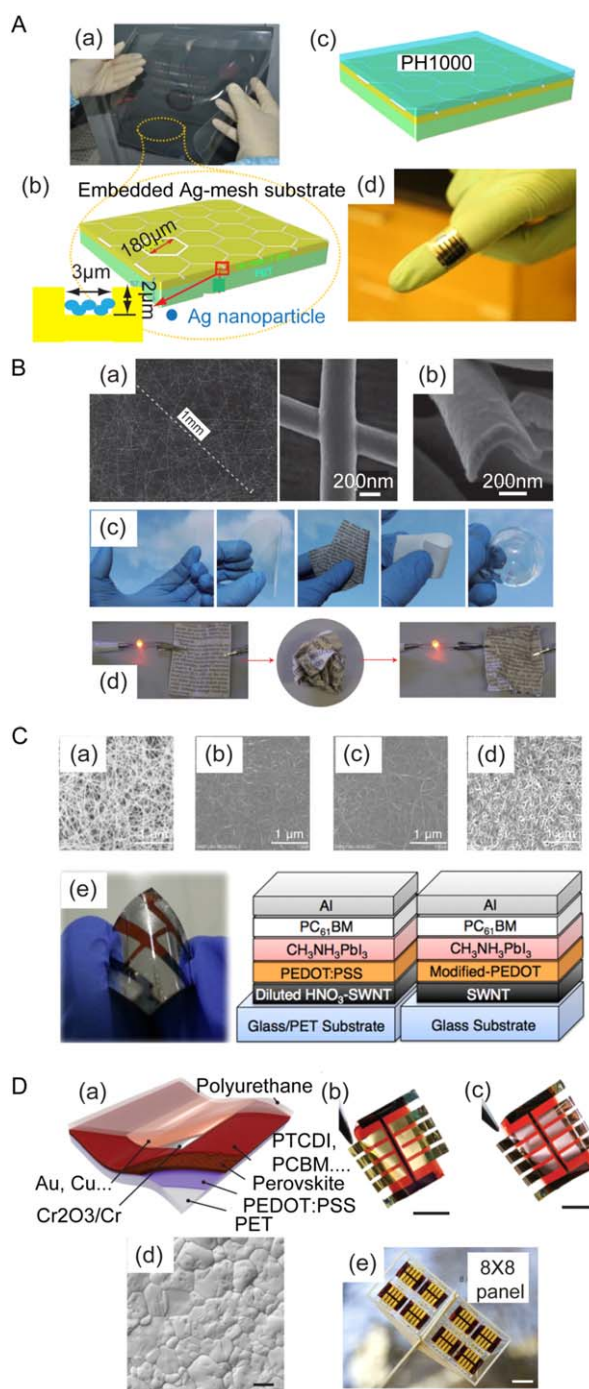
Figure 14. (A) Schematic illustration of the flexible PET substrate with embedded Ag-mesh (FEAMs) substrate and hybrid electrode. (a) An image of the large-area FEAMs substrate. (b) The structure of the FEAMs substrate with detail parameters. (c) Diagram of the hybrid electrode PET/Ag-mesh/PH1000. (d) PET/Ag-mesh/ PH1000/ PEDOT: PSS/MAPbI$_3$/PCBM/Al solar cell [105]. Copyright 2016, Nature Publishing Group. (B) Metal nanotrough network. (a) Top-view SEM images of gold nanotrough networks (left) and a junction between two nanotroughs (right). (b) SEM image of the cross-section of a single gold nanotrough, revealing its concave shape. (c) Gold nanotrough networks can be transferred easily onto various substrates, including a glass slide, PET plastic, paper, textile and a curved glass flask (left to right). (d) Photographs of 'conducting paper', fabricated by transferring gold nanotrough networks onto paper. After crushing and unfolding, the paper remained conducting (resistance increasing from 73 V to 131 V) [107]. Copyright 2013, Nature Publishing Group. C) SEM images of (a) SWCNTs; (b) IPA-PEDOT: PSS on SWCNTs; (c) surfactant-PEDOT: PSS on SWCNTs; (d) PEDOT: PSS on HNO$_3$-doped SWCNTs, and (e) ITO/PEDOT: PSS, SWCNT/modified-PEDOT:PSS, SWCNT/surfactant-PEDOT: PSS solar cell [108]. Copyright 2015, American Chemical Society. (D) Ultra-thin and light PSCs. (a) Schematic of the solar cell stack. (b) freestanding 3-μm-thick solar cells with gold top metal. Scale bar, 1 cm. (c) Perovskite solar foil with low-cost copper back contacts. Scale bar, 1 cm. (d) SEM image of MAPI film on PEDOT: PSS-coated foil, revealing tightly packed crystallites of several micrometers in size. Scale bar, 1 μm. (e) Close-up photograph of the horizontal stabilizer with integrated solar panel. Scale bar, 2 cm [109]. Copyright 2015, Nature Publishing Group.

Sun *et al* [110] used PEDOT: PSS to replace ITO, and at the same time PEDOT: PSS also as a HTL. In order to improve the electrical conductivity of PEDOT: PSS, they used mesylate (MSA) to process the PEDOT: PSS membrane obtained by spin coating. The PCE of the obtained flexible device is 8.1%, and it
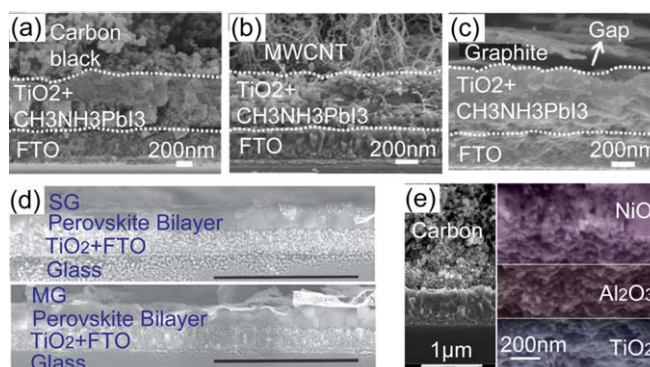
Figure 15. Cross sectional structure of the C-PSCs based on different carbon electrodes: (a) carbon black electrode [111]; copyright 2015, Royal Society of Chemistry. (b) Carbon nanotube electrode [111]; copyright 2015, Royal Society of Chemistry. (c) Graphite electrode [111]; copyright 2015, Royal Society of Chemistry. (d) Graphene electrode [112]; copyright 2015, Wiley-VCH. (e) Carbon black/graphite electrode [113]; copyright 2015, Elsevier.

remains basically stable after 2000 bends. Kaltenbrunner *et al* [109] used PEDOT: PSS to replace ITO on the PET substrate and at the same time it served as a HTL. The ETL was modified by Cr_2O_3 to prevent direct contact between the metal counter electrode and the perovskite layer, and finally prepared the flexible calcium ultra-thin PSCs with a total thickness of $3\mu m$. Their PCE exceeds 12%, and they have a power density of 23 W g^{-1} and good flexibility (as shown in figure 14(D)). This provides a new idea for the property modification of PEDOT: PSS solution printed thin films.

3.4.2. Printable counter electrode materials
Yang *et al* [114] prepared a AgNW which has excellent dispersive compounds; the PSC's top electrode of the AgNW was prepared by spray coating, and the PCE of the PSCs achieved 10.64%. Xie *et al* [115] modified a AgNW to prepare polyethylenimine (PEI)/AgNW ink, and used inkjet printing to prepare it into the PSC's top electrode, improving the PCE of the PSCs to 14.17%. In addition, Ni and Cu metal nanowires have also been successfully used to prepare transparent conductive electrodes [116, 117].

However, the disadvantage of metal nanowires being utilized as the top electrode of the PSCs is that the polar solvent used to disperse the nanowires will degrade the perovskite layer below. There are two solutions to this problem: one is the use of non-polar solvents [34, 118, 119] and the other is the use of a network of mechanically transferred metal nanowires as the top electrode [120–122].

3.4.3. Carbon electrodes
Wei *et al* [123] developed a large-area inkjet printing technology for carbon black carbon electrode deposition. In their research, they developed targeted 'in situ chemical transformation technology': CH_3NH_3I was introduced into carbon black ink to strengthen the combination of the carbon electrode and perovskite film through a rapid reaction between CH_3NH_3I and PbI_2

during printing deposition; this type of printing technology for C-PSCs provides a possibility for accurate and large-area deposition of carbon electrodes.

Wei *et al* [111] studied the preparation of carbon electrodes using a variety of carbon materials (carbon black, graphite and carbon nanotubes), as shown in figure 15(a-c). Due to the large size of flake graphite, the film-forming quality of the carbon electrode decreases, and the connection between graphite is poor and cannot form close contact with perovskite, which leads to the degradation of PSCs' performance. Because of the small size and good flexibility of the one-dimensional carbon nanotubes, the film quality of the carbon paste can be improved by adding the carbon nanotubes to the carbon paste. The prepared carbon electrode has the characteristics of high mechanical strength and fast charge transfer. Recently, the Fermi level of carbon nanotubes has been reduced by doping carbon nanotubes with B element, making them better match with the perovskite valence band, which significantly enhances the transfer rate of holes at the interface and significantly improves the PCE to 15.2% [124].

Yan *et al* [112] applied graphene to the preparation of C-PSCs (as shown in figure 15d), and thin and flexible graphene made it more closely bond to perovskite film. By controlling the number of layers of graphene, the Fermi energy level can be adjusted to better match the perovskite valence band energy level, effectively enhancing the transfer of interface holes. Compared with single-layer graphene (SG), multi-layer graphene (MG) has more matching Fermi levels, resulting in better hole mobility and higher PCE (11.5% versus 6.7%).

Wei *et al* [125] obtained the PSCs of the $TiO_2/MAPbI_3/C$ structure without a HTL by hot pressing the low-temperature sintered thermoplastic carbon electrode coated on Teflon to the perovskite layer prepared by a two-step method, and achieved a PCE of 13.53%. Wang *et al* [113, 126] took carbon as the counter electrode, and inserted Al_2O_3 and NiO

space layers into the carbon electrode and TiO_2 porous layer, as shown in figure 15(e). The PCE of PSCs achieved 15.03%.

Chang *et al* [127] mixed carbon black, graphite and macromolecular binder and prepared carbon slurry, which can be used to deposit a carbon electrode at low temperature. The electrode can be directly deposited on the prepared perovskite film to form brush-type C-PSCs. Due to the deposition of perovskite film and carbon electrode respectively, there are many parameters that can be regulated in the preparation process of perovskite film, and the traditional HTM-PSCs deposition method can also be used to prepare high-quality film, so that the brush-type C-PSCs have good prospects. Currently, based on the commercialization of conductive carbon slurry, the PCE of C-PSCs achieved 14.5%.

4. Conclusions and prospects

In recent years, PSCs have received extensive attention from both scientific and industrial circles. One important reason for this is that the record PCE of PSCs has exceeded 24.2%, which is close to silicon solar cells. Although the PSC shows its potential already, its scaling up technologies, e.g. printing, are becoming bottlenecks for its commercialization. Printing is solution processable, however, not all solution processable materials can be efficiently printed. We reviewed the most recently published paper about printing whole or parts of PSCs and summarized these printing-friendly materials including: perovskite materials (with or without additives), charge-transporting materials (ETM and HTM) and electrodes:

(1) Perovskite materials: at present, most research is focused on stability and bandgap adjustment of perovskite materials themselves, however, only a few works discuss their properties for printing technologies. Developing printing technology-related processing technologies, and introducing new additives or solvents will be the most important areas for future research on printed PSCs.

(2) Charges transporting materials: most in used charge-transporting materials are processed through evaporating or spin coating, which are different to printing technologies. Developing printable materials/inks and printing-related techniques will be important concerns for the future development of charge-transporting materials.

(3) Electrodes: gold is one of the most widely used stable and high-performance electrodes for high-performance PSCs, however, it is undesirable for the photovoltaic industry. Carbon-based electrodes, stable printable metal electrodes/composite

electrodes etc are becoming the new research focus in fully printed PSCs.

ORCID iDs

Yong Peng ⓘ https://orcid.org/0000-0002-4543-8212

References

[1] Kojima A *et al* 2009 *J. Am. Chem. Soc.* **131** 6050–1
[2] Kim H S *et al* 2012 *Sci. Rep.* **2** 591
[3] Lee M M *et al* 2012 *Science* **338** 643–7
[4] Burschka J *et al* 2013 *Nature* **499** 316–9
[5] Tsai H *et al* 2016 *Nature* **536** 312–6
[6] Ummadisingu A *et al* 2017 *Nature* **545** 208–12
[7] Han Q *et al* 2018 *Science* **361** 904–8
[8] Best research-cell efficiency chart *National Renewable Energy Laboratory* (https://nrel.gov/pv/cell-efficiency.html)
[9] Cheng Y B *et al* 2016 *Nature* **539** 488–9
[10] Wang F *et al* 2018 *Adv. Funct. Mater.* **28** 1803753
[11] Zhou H *et al* 2014 *Science* **345** 542–6
[12] Liu M, Johnston M B and Snaith H J 2013 *Nature* **501** 395–8
[13] Jeon N J *et al* 2014 *Nat. Mater.* **13** 897–903
[14] Oku T 2015 *Solar Cells* (Rijeka: InTech) (https://doi.org/10.5772/58490)
[15] Colella S E *et al* 2013 *Chem. Mater.* **25** 4613–8
[16] Lee J W *et al* 2014 *Adv. Mater.* **26** 4991–8
[17] Shao Y C *et al* 2014 *Nat. Commun.* **5** 5784
[18] Li G *et al* 2005 *Nat. Mater.* **4** 864–8
[19] Li G, Zhu R and Yang Y 2012 *Nat. Photonics* **6** 153–61
[20] Zhang M and Zhan X 2019 *Adv. Energy Mater.* **9** 1900860
[21] Ke W J *et al* 2014 *Appl. Mater. Interfaces* **6** 15959–65
[22] Ouyang M *et al* 2008 *J. Phys. Chem. C* **112** 11250–6
[23] Ke W J *et al* 2015 *J. Am. Chem. Soc.* **137** 6730–3
[24] Ke W J *et al* 2015 *J. Mater. Chem. A* **3** 24163–8
[25] Qin M C *et al* 2016 *ACS Appl. Mater. Interfaces* **8** 8460–6
[26] Liu D and Kelly T L 2014 *Nat. Photonics* **8** 133–8
[27] Heo J H *et al* 2016 *J. Mater. Chem. A* **4** 1572–8
[28] Jeon N J *et al* 2014 *J. Am. Chem. Soc.* **136** 7837–40
[29] Conings B *et al* 2014 *Adv. Mater.* **26** 2014–46
[30] Jung E H *et al* 2019 *Nature* **567** 511–5
[31] Chavhan S *et al* 2014 *J. Mater. Chem. A* **2** 12754–60
[32] Chen W *et al* 2015 *Science* **350** 944–8
[33] Liu Z H *et al* 2015 *Dalton Trans.* **44** 3967–73
[34] Guo F *et al* 2015 *Nanoscale* **7** 1642–9
[35] You P *et al* 2015 *Adv. Mater.* **27** 3632–8
[36] Mei A *et al* 2014 *Science* **345** 295–8
[37] Javier U M *et al* 2018 *Chem. Mater.* **31** 6435–42
[38] Yin X X *et al* 2017 *Nano Energy* **40** 163–9
[39] Xu B *et al* 2017 *Chem* **2** 676–87
[40] Xu B *et al* 2016 *Energy Environ. Sci.* **9** 873–7
[41] Bi D *et al* 2016 *Nano Energy* **23** 138–44
[42] Qin T S *et al* 2017 *Nano Energy* **31** 210–7
[43] Sun L *et al* 2016 *Chem. Sci.* **7** 2633–8
[44] Zhang J *et al* 2016 *Adv. Energy Mater.* **6** 1502536

[45] Christians J A *et al* 2018 *Nature Energy* **3** 68–74
[46] Azmi R *et al* 2018 *Nano Energy* **44** 191–8
[47] Zhang H *et al* 2018 *Chem. Sci.* **9** 5919–28
[48] Huang C *et al* 2016 *J. Am. Chem. Soc.* **138** 2528–31
[49] Paek S *et al* 2017 *Adv. Mater.* **35** 1606555
[50] Malinauskas T *et al* 2016 *Energy Environ. Sci.* **9** 1681–6
[51] Saliba M *et al* 2016 *Nature Energy* **1** 15017
[52] Sun Y H *et al* 2018 *Solar RRL* **2** 1700175
[53] Reddy S S *et al* 2017 *Nano Energy* **41** 10–7
[54] Hu L *et al* 2017 *ACS Appl. Mater. Interfaces* **9** 43902–9
[55] Xiao J *et al* 2015 *Adv. Energy Mater.* **5** 1401943
[56] Yang W S *et al* 2017 *Science* **356** 1376–9
[57] Zhang F *et al* 2016 *Nano Energy* **20** 108–16
[58] Jiang X Q *et al* 2019 *Adv. Energy Mater.* **9** 1803287
[59] Wang J M *et al* 2018 *Adv. Energy Mater.* **8** 1701688
[60] Cho K T *et al* 2017 *Adv. Energy Mater.* **7** 1601733
[61] Chen S *et al* 2017 *ACS Appl. Mater. Inter.* **9** 13231–9
[62] Yin X *et al* 2016 *ACS Nano* **10** 3630–6
[63] Jung J W, Chueh C C and Jen A K Y 2015 *Adv. Mater.* **27** 7874–80
[64] Zhang H *et al* 2018 *Adv. Energy Mater.* **8** 1702762
[65] Arora N *et al* 2017 *Science* **358** 768–71
[66] Koo B *et al* 2016 *Adv. Funct. Mater.* **26** 5400–7
[67] Lei H *et al* 2017 *Solar RRL* **1** 1700038
[68] Sun W *et al* 2016 *Nanoscale* **8** 10806–13
[69] Li X *et al* 2017 *ACS Appl. Mater. Interfaces* **9** 41354–62
[70] Wu Y Z *et al* 2017 *Adv. Mater.* **29** 1701073
[71] Razza S *et al* 2015 *J. Power Sources* **277** 286–91
[72] Deng Y H *et al* 2018 *Nature Energy* **3** 560–6
[73] Jung Y S *et al* 2017 *ACS Appl. Mater. Interfaces* **9** 27832–8
[74] Wang C *et al* 2018 *Sol. RRL* **2** 1700209
[75] Turren-Cruz S H, Hagfeldt A and Saliba M 2018 *Science* **362** 449–53
[76] Feng J S *et al* 2018 *Adv. Mater.* **30** 1801418
[77] Zhang Y *et al* 2017 *Adv. Mater.* **29** 1702157
[78] Liu X *et al* 2016 *Nano Energy* **30** 417–25
[79] Wu Z F *et al* 2018 *Adv. Mater.* **30** 1703670
[80] Wei J *et al* 2016 *Nano Energy* **26** 139–47
[81] Bi D Q *et al* 2018 *Nat. Commun.* **9** 4482
[82] Yu J C *et al* 2019 *Adv. Mater.* **31** 1805554
[83] Yang F *et al* 2018 *Angew. Chem. Int. Ed.* **57** 12745–9
[84] Liang J *et al* 2017 *J. Am. Chem. Soc.* **139** 14009–12
[85] Xiang W C *et al* 2019 *Joule* **3** 1–10

[86] Liu G *et al* 2019 *Adv. Funct. Mater.* **29** 180756
[87] Ye T *et al* 2018 *Adv. Funct. Mater.* **28** 1801654
[88] Li P *et al* 2018 *Adv. Mater.* **30** 1805323
[89] Grancini G *et al* 2017 *Nat. Commun.* **8** 15684
[90] Yavari M *et al* 2018 *Adv. Energy Mater.* **8** 1800177
[91] Bu T *et al* 2017 *Adv. Energy Mater.* **7** 1700576
[92] Bu T L *et al* 2018 *Nat. Commun.* **9** 4609
[93] Wei J *et al* 2018 *ACS Nano* **12** 5518–29
[94] Song S *et al* 2018 *Nano Energy* **49** 324–32
[95] Li Y *et al* 2016 *J. Mater. Chem. A* **4** 10130–4
[96] Kim H I *et al* 2018 *Adv. Energy Mater.* **8** 1702872
[97] Zhao D B *et al* 2016 *Angew. Chem. Int. Ed.* **55** 8999–9003
[98] Sun C *et al* 2016 *Adv. Energy Mater.* **5** 1501534
[99] Chen C *et al* 2018 *ACS Appl. Mater. Interfaces* **10** 38970–7
[100] Wang Y *et al* 2015 *ACS Appl. Mater. Interfaces* **7** 7170–9
[101] Gao W *et al* 2017 *Adv. Funct. Mater.* **27** 1703938
[102] Hu X *et al* 2017 *Adv. Mater.* **29** 1703236
[103] Yang I S *et al* 2017 *Nano Energy* **32** 414–21
[104] Li B *et al* 2015 *Nano Lett.* **15** 6722–6
[105] Li Y W *et al* 2016 *Nature Commun.* **7** 10214
[106] Xiong W W *et al* 2016 *Adv. Mater.* **28** 7167–72
[107] Wu H *et al* 2013 *Nat. Nanotech.* **8** 421–5
[108] Jeon I *et al* 2015 *Nano Lett.* **15** 6665–71
[109] Kaltenbrunner M *et al* 2015 *Nat. Mater.* **14** 1032–9
[110] Sun K *et al* 2015 *ACS Appl. Mater. Interfaces* **7** 15314–20
[111] Wei Z H *et al* 2015 *J. Mater. Chem. A* **3** 24226–31
[112] Yan K Y *et al* 2015 *Small* **11** 2269–74
[113] Cao K *et al* 2015 *Nano Energy* **17** 171–9
[114] Yang K *et al* 2016 *Nanotechnology* **27** 095202
[115] Xie M *et al* 2018 *Sol. RRL* **2** 1700184
[116] Bryant D *et al* 2014 *Adv. Mater.* **26** 7499–504
[117] Hwang H *et al* 2016 *Adv. Funct. Mater.* **26** 6545–54
[118] Leem D S *et al* 2011 *Adv. Mater.* **23** 4371–5
[119] Zhang J *et al* 2016 *Appl. Surf. Sci.* **369** 308–13
[120] Eperon G E *et al* 2015 *J. Phys. Chem. Lett.* **6** 129–38
[121] Spyropoulos G D *et al* 2016 *Energy Environ. Sci.* **9** 2302–13
[122] Ahn J *et al* 2017 *Adv. Energy Mater.* **7** 1602751
[123] Wei Z *et al* 2014 *Angew Chem* **53** 13239–43
[124] Zheng X *et al* 2017 *Nano Lett.* **17** 2496–505
[125] Wei H *et al* 2015 *Carbon* **93** 861–8
[126] Xu X *et al* 2015 *Nano Lett.* **15** 2402–8
[127] Chang X *et al* 2016 *ACS Appl. Mater. Inter.* **8** 30184–92